An assessment of geographical distribution of different plant functional types over North America simulated using the CLASS-CTEM modelling framework

Rudra K. Shrestha[1], Vivek K. Arora[1], Joe R. Melton[2], and Laxmi Sushama[3]

[1]Canadian Centre for Climate Modelling and Analysis, Environment and Climate Change Canada, University of Victoria, Victoria, BC, V8W 2Y2, Canada

[2]Climate Research Division, Environment and Climate Change Canada, Toronto, Ontario, Canada

[3]Département des sciences de la Terre et de l'atmosphère, Université du Québec à Montréal, Canada

Correspondence to: V. K. Arora (Vivek.Arora@canada.ca)

Abstract

The performance of the competition module of the CLASS-CTEM (Canadian Land Surface Scheme and Canadian Terrestrial Ecosystem Model) modelling framework is assessed at 1° spatial resolution over North America by comparing the simulated geographical distribution of its plant functional types (PFTs) with two observation-based estimates. The model successfully reproduces the broad geographical distribution of trees, grasses and bare ground although limitations remain. In particular, compared to the two observation-based estimates, the simulated fractional vegetation coverage is lower in the arid south-west North American region and higher in the Arctic region. The lower than observed simulated vegetation coverage in the south-west region is attributed to lack of representation of shrubs in the model and plausible errors in the observation-based data sets. The observation-based data indicates vegetation fractional coverage of more than 60% in this arid region, despite only 200-300 mm of precipitation that the region receives annually and observation-based leaf area index (LAI) values in the region are lower than one. The higher than observed vegetation fractional coverage in the Arctic is likely due to the lack of representation of moss and lichen PFTs and also likely because of inadequate representation of permafrost in the model as a result of which the C_3 grass PFT performs overly well in the region. The model generally reproduces the broad spatial distribution and the total area covered by the two primary tree PFTs (needleleaf evergreen and broadleaf cold deciduous

trees) reasonably well. The simulated fractional coverage of tree PFTs increases after 1960s in response to the CO_2 fertilization effect and climate warming. Differences between observed and simulated PFT coverages highlight model limitations and suggest that the inclusion of shrubs, and moss and lichen PFTs, and an adequate representation of permafrost will help improve model performance.

1 Introduction

The terrestrial ecosystem plays an important role in regulating climate and weather through land-atmosphere exchange of water and energy (Cramer et al., 2001; Garnaud et al., 2015; Pielke et al., 1998; Ran et al., 2016) and in mitigating climate change by sequestering atmospheric CO_2 (Bonan, 2008; Timmons et al., 2016). The projected sink of atmospheric CO_2 is uncertain due to disagreements among the Earth system models (ESMs) (Arora et al., 2013; Friedlingstein et al., 2006) primarily due to differing responses of their terrestrial ecosystem modules to future changes in atmospheric CO_2. This uncertainty arises primarily because of the differences in the strength of the CO_2 fertilization effect on the land carbon cycle components (Arora et al., 2013; Cramer et al., 2001; Friend et al., 2013) but also because of differences in the response of vegetation. Models differ in how the spatial distribution of vegetation, and its composition, changes in response to changing climate and increasing CO_2 (Cramer et al., 2001). These differences are also resolution dependent. For example, models with coarse grid resolutions cannot explicitly resolve climatic niches, which in turn potentially contributes to biases in simulated vegetation distribution (Melton and Arora, 2016; Shrestha et al., 2016).

Vegetation responds to changes in climate and atmospheric CO_2 concentration by changing its structural attributes including leaf area index (LAI), rooting depth, vegetation height, and canopy mass, as well as its areal extent. Structural vegetation changes generally occur over seasonal to decadal time scales (Kramer and Kozlowski, 1979), while the slower areal extent changes typically occur on decadal to centennial time scales (Ritchie and Macdonald, 1986). The dynamic behavior of vegetation affects weather and climate due to its strong control over biophysical processes. At hourly to daily timescales, vegetation affects the exchange of water and energy between the land surface and the atmosphere primarily through the control of leaf stomata. At longer seasonal, annual and decadal timescales, vegetation affects components of energy and water balance through its structure (LAI, rooting depth, etc.) and its areal extent and thereby land surface albedo. Conversely, dynamics of vegetation is directly influenced by climate and the competitive ability of the plants. In this way vegetation responds to climate by changing its structure and areal extent depending on the colonization ability of plants. These

climate-vegetation interactions have been well documented (e.g. Gobron et al., 2010; Wang et al., 2011).

Natural vegetation is typically characterized in dynamic global vegetation models (DGVMs) based on a limited number of PFTs (Sitch et al., 2003) because it is impossible to represent thousands of species in a model. Species characterized by similar attributes, mainly based on their form and interactions with the environment (Box, 1996), are grouped together as a single PFT. For example, tree species with similar leaf form such as fir *(Abies)*, spruce *(Picea)* and pine *(Pinus)* are classified as needleleaf evergreen trees. The geographical distribution of the PFTs in DGVMs is determined by their ability to grow and increase their areal extent given certain climate and soil conditions and their competitive ability.

One way of representing competition between PFTs in DGVMs is through the use of the Lotka-Volterra (LV) equations. While originally developed for predator-prey competition, the LV equations have been used in a number of DGVMs (Arora and Boer, 2006; Brentnall et al., 2005; Cox, 2001; Zhang et al., 2015). The use of the classical form of the LV equations for modelling competition between PFTs, however, leads to an amplified expression of dominance in that the dominant PFT ends up occupying a disproportionately large fraction of a grid cell leading to little co-existence between PFTs. Arora and Boer (2006) proposed changes to the classical implementation of the LV equations for modelling competition between PFTs to reduce this amplified expression of dominance. Their approach, which has been implemented in the CLASS-CTEM modelling framework and which allows improved co-existence of PFTs compared to the classical LV equations, has been shown to simulate vegetation distribution reasonably well at the global (Melton and Arora, 2016) as well as point (Shrestha et al., 2016) scales. Both these studies used climate averaged over ~3.75° spatial resolution. The CLASS-CTEM framework consists of the Canadian Land Surface Scheme (CLASS) coupled to the Canadian Terrestrial Ecosystem Model (CTEM) which is a dynamic vegetation model.

In this paper, we evaluate the competition module of the CLASS-CTEM modelling framework at the regional scale over the North American domain at 1° spatial resolution. This resolution is much finer than the 3.75° resolution used in the Melton and Arora (2016) study and therefore in

principle should allow a more realistic simulation of geographical distribution of PFTs as climate niches are resolved.

The rest of this paper is organized as follows: Section 2 describes the CLASS-CTEM modelling framework, details of the observation-based data and the experimental setup. Results are presented in section 3 and a discussion follows in section 4. Finally, a summary and conclusions are provided in section 5.

2 Model, data and methods

2.1 CLASS-CTEM model

The results presented here are obtained by coupling version 2.0 of CTEM (Melton and Arora, 2016), which dynamically simulates fractional coverage of its PFTs, to version 3.6 of CLASS (Verseghy et al., 1993). CTEM simulates terrestrial processes for seven non-crop and two crop PFTs (Table 1) and prognostically tracks carbon in three living vegetation components (leaves, stems and roots) and two dead carbon pools (litter and soil). The terrestrial ecosystem processes simulated in this study include photosynthesis, autotrophic respiration, heterotrophic respiration, dynamic leaf phenology, allocation of carbon from leaves to stem and root components, fire, land use change, and competition between PFTs which dynamically determines the fractional coverage of each PFT. The amount of carbon in the leaf, stem and root components is used to estimate structural attributes of vegetation. LAI is calculated from leaf biomass using PFT-dependent specific leaf area (SLA) which determines area of leaves that can be constructed per kg C of leaf biomass (Arora and Boer, 2005); vegetation height is calculated based on stem biomass for tree PFTs and LAI for grass PFTs; and rooting depth is calculated based on root biomass (Arora and Boer, 2003). CTEM operates at a time step of one day except for photosynthesis and leaf respiration which are calculated every 30 minutes for consistency with CLASS' energy and water balance calculations which require stomatal resistance calculated by the photosynthesis module of CTEM.

CLASS simulates the energy and water balance components at the land surface and operates at a 30 minutes time step. Liquid and frozen soil moisture and soil temperature are evaluated for three soil layers (with maximum thicknesses of 0.1, 0.25 and 3.75 m). The actual thicknesses of these permeable soil layers are determined by the depth to bedrock, which is specified on the basis of the global data set of Zobler (1986). CLASS distinguishes four PFTs (needleleaf trees, broadleaf trees, crops and grasses) which map directly to the nine PFTs represented in CTEM as shown in Table 1. Needleleaf trees in CTEM are divided into deciduous and evergreen types, broadleaf trees are divided into cold and drought deciduous and evergreen types, and crops and grasses are divided into C_3 and C_4 types based on their photosynthetic pathways. In coupled mode, CLASS uses the dynamically simulated vegetation attributes (including LAI, vegetation height, canopy mass and rooting depth) and stomatal resistance calculated by CTEM, and CTEM uses the soil moisture, soil temperature and net shortwave radiation calculated by CLASS. The coupling frequency between CLASS and CTEM is one day.

2.1.1 **Competition parameterization**

Competition between PFTs in CTEM is parameterized following Arora and Boer (2006) who presented a modified version of the LV equations. The approach is described in detail by Melton and Arora (2016) and briefly summarized here. Consider, for simplicity, two PFTs that exist in a grid cell with fractional coverages f_1 and f_2. Let PFT 1 represent a tree PFT and PFT 2 represent a grass PFT. The bare fraction of grid cell not covered by any vegetation is represented by f_B. As a result, $f_1 + f_2 + f_B = 1$. The rate of change of fractional coverages of the two PFTs and bare fraction, for this example, are given by,

$$\frac{df_1}{dt} = c_1 f_1^{\beta}(1 - f_1) - m_1 f_1 \quad (1)$$

$$\frac{df_2}{dt} = c_2 f_2^{\beta}(1 - f_1 - f_2) - c_1 f_1^{\beta} f_2 - m_2 f_2 \quad (2)$$

$$\frac{df_B}{dt} = -c_1 f_1^{\beta} f_B - c_2 f_2^{\beta} f_B + m_1 f_1 + m_2 f_2 \quad (3)$$

where c_1, c_2 and m_1, m_2 are the colonization and mortality rates for PFT 1 and PFT 2, respectively. Colonization and mortality rates cannot be negative. Equations (1) and (2) show that PFT 1 can invade the fraction covered by PFT 2 and the bare fraction; and that PFT 2 can only invade the bare fraction. PFT 2 is not allowed to invade the fraction covered by PFT 1 because it is ranked lower than PFT 1. In CTEM, the superiority or ranking of the seven natural non-crop PFTs is based on the tree-grass distinction and their colonization rates. Trees are always considered to be superior than grasses because of their ability to shade them (Siemann and Rogers, 2003). Within the tree and grass PFTs the dominance is determined dynamically based on the colonization rate. The exponent β ($0 \leq \beta \leq 1$), an empirical parameter, controls the behaviour of the LV equations. For $\beta = 1$, the equations represent the classical form of the LV equations. The equilibrium fractional coverages for PFT 1 and 2 and bare fraction for this classical form of the LV equations, denoted by $\tilde{f}_1, \tilde{f}_2$ and are given by,

$$\tilde{f_1} = \max\left\{\left(\frac{c_1 - m_1}{c_1}\right), 0\right\} \quad (4)$$

$$\tilde{f_2} = \max\left\{\left(\frac{(c_2 - m_2) - \left(1 + \frac{c_2}{c_1}\right)(c_1 - m_1)}{c_2}\right),\ 0\right\} \quad (5)$$

$$\tilde{f_B} = \frac{(m_1 \tilde{f_1} + m_2 \tilde{f_2})}{(c_1 \tilde{f_1} + c_2 \tilde{f_2})} \quad (6)$$

In equations (1) and (2), if the fractional coverages of PFT 1 and PFT 2 are initially zero then the PFTs cannot expand for β = 1, implying that a minimum seeding fraction is always required. Furthermore, in equation (5) as long as (c_1–m_1) is greater than (c_2–m_2) then the equilibrium solution for f_2 will always be zero and PFT 2 will not be able to coexist with PFT 1. These features of the classical form of the LV equations are avoided when $\beta = 0$, following Arora and Boer (2006). The equilibrium fractional coverages for PFT 1 and 2 and bare fraction for the case with $\beta = 0$ are given by,

$$\tilde{f_1} = \left(\frac{c_1}{c_1 + m_1}\right) \quad (7)$$

$$\tilde{f_2} = \frac{c_2(1 - \tilde{f_1})}{(c_1 + c_2 + m_2)} = \left(\frac{c_2 m_1}{(c_1 + m_1)(c_1 + c_2 + m_2)}\right) \quad (8)$$

$$\tilde{f}_B = \frac{(m_1 \tilde{f}_1 + m_2 \tilde{f}_2)}{(c_1 + c_2)} \quad (9)$$

Unlike the classical version of the LV equations, the modified version of the equations with $\beta = 0$ does not require a minimum seeding fraction, and PFTs are able to increase their areal extent as long as the climate is favorable and c_i is positive. Also, as long as $m_1 > 0$ and $c_2 > 0$ then PFT 2 is able to coexist at equilibrium with PFT 1. Other values of β between 0 and 1 give the dominant PFT varying levels of access to sub-dominant PFTs but coexistence is most possible in the case with $\beta = 0$.

The calculations of colonization and mortality rates are described in detail in Melton and Arora (2016). Briefly, the colonization rate depends on the net primary productivity of a PFT. The better a PFT performs for given climatic and soil conditions; the higher is its colonization rate. The mortality rate represents the combined effect of four different processes: intrinsic or age-related mortality, growth or stress mortality, mortality due to disturbance, and mortality due to adverse climate which ensures that tree PFTs do not venture outside their bioclimatic zones.

2.2 Forcing data

The Climate Research Unit – National Centre for Environmental Prediction (CRU-NCEP) reanalysis dataset (Viovy, 2012), is used to drive the model. The meteorological variables (surface temperature, pressure, precipitation, wind, specific humidity, and incident short-wave and long-wave radiation fluxes) are available at a spatial resolution of 0.5° × 0.5° and at a six hourly time interval for the period 1901-2010. These data are interpolated to 1° resolution spatially, and disaggregated to half-hourly time resolution, a standard CLASS-CTEM model integration time step. Temperature, pressure, wind, specific humidity, and long-wave radiation are linearly interpolated in time while short-wave radiation is assumed to change with the solar zenith angle with maximum radiation occurring at solar noon. Following Arora (1997), the six-hourly precipitation amount (P, mm/6-hour) is used to estimate the number of wet half-hours (w_h) in a given six-hour period for $P > 0$ as

$$w_h = \text{integer}(\max[1, \min(12, 2.6 \log(6.93\, P))]). \quad (10)$$

The total precipitation amount is then distributed randomly but conservatively over these wet half-hours. For instance, if seven out of 12 half hours intervals are calculated to be wet using equation (10) then seven random numbers varying between 0 and 1 are generated and the six-hourly precipitation amount is divided into seven parts in proportion to their respective random numbers

Figure 1 shows the spatial distribution of mean annual precipitation and surface temperature over the North American domain considered in this study. Mean annual precipitation values range from less than 200 mm in the arid south-west United States and the high Arctic to more than 1500 mm on the Pacific coast. Mean annual temperature varies from around 24° C near the southern limit of the domain in Mexico to less than -20° C in the Arctic tundra.

2.3 Observation-based data

2.3.1 Fractional coverage of PFTs

Observation-based estimates of fractional coverages of PFTs are based on a modified version of the Wang et al. (2006) data set (hereafter WANG06) and the Moderate Resolution Imaging Spectroradiometer land cover product (Friedl et al., 2013) (hereafter MODIS). These data are used to evaluate the model results.

The WANG06 data set was developed for use by CTEM in simulations in which competition is turned off and prescribed fractional coverage of PFTs is used. It combines observation- and model-based data to estimate the annual change in fractional coverage of CTEM's nine PFTs from 1850 to 2000. The Global Land Cover for the year 2000 (GLC2000), which is considered as a base year for environmental assessment, divides the global land cover in 22 types is available at 1 km resolution. WANG06 (their Table 2) mapped the GLC2000 data to CTEM's nine PFTs aggregated to 0.5° resolution. The GLC2000 data were then extrapolated back to 1850 by adjusting the changes in crop area based on the then available Ramankutty and Foley (1999) crop data set. Here, we use a modified version of the WANG06 data set which is based on the

HYDE v.3.1 crop data set (Hurtt et al., 2011) and generate an estimate of fractional coverage of CTEM PFTs for the period 1850-2012.

The MODIS data set is based on the International Geosphere-Biosphere Programme (IGBP) global vegetation data and University of Maryland's Science Data Set classification schemes at 0.25° spatial resolution. The data are derived from NASA HDF-EOS MODIS/Terra land cover type. The data set is for the period 2001 to 2014 and contains 17 land cover types which we map to CTEM's nine PFTs following the logic used in Wang et al. (2006) as shown in Table 2. The fractional coverage of each of the nine CTEM PFT is first obtained at 0.25 degree resolution for each year using the mapping scheme described in Table 2. These fractional coverages are then re-gridded to the 1° spatial resolution for individual years. Finally, the data are averaged over the period 2001-2014 to evaluate model results. MODIS data are known to exhibit substantial interannual variability. Broxton et al. (2014), for instance, report that globally 40% of land pixels show land cover change one or more times during 2001–2010 period. This does not necessarily indicate changes in land cover but rather these differences are due to low accuracy in categorizing the remotely sensed vegetation into one of the 17 MODIS land cover types, as Broxton et al. (2014) note. This low accuracy is itself attributed to the fact that many landscapes include mixtures of vegetation classes. Our re-gridding of fractional coverages to 1° spatial resolution and averaging over the 2001-2014 time period to obtain climatology of land cover alleviates some of the uncertainty since the effect of inaccurately classified land cover categories is reduced due to both spatial and temporal averaging.

The separation of the broadleaf deciduous PFT into its drought and cold deciduous components is performed via the approach used by WANG06. They assumed that below 24 °N deciduousness is caused by soil moisture limitation and hence all broadleaf deciduous trees below this latitude are drought deciduous, and above 34 °N deciduousness is caused by low temperatures and so all broadleaf deciduous trees above this latitude are cold deciduous. Between 24 °N and 34 °N, following WANG06 we assume a linear transition from drought deciduous to cold deciduous trees. Finally, the separation of grasses into their C_3 and C_4 components is based on the geographical distributions of the C_3 and C_4 fractions in the WANG06 data set.

2.3.2 **Gross primary productivity and LAI**

Observation-based estimates of gross primary productivity (GPP) are based on Beer et al. (2010). These data are based on the ecosystem level GPP obtained using eddy covariance measurements from more than 250 stations across the globe. Beer et al. (2010) extrapolated GPP values based on these eddy covariance flux data to the global scale using diagnostic models for the period 1982 – 2008, and the average over this time period is used to evaluate the model results. LAI data used for validation are the same as those used by Anav et al. (2013) and are based on Zhu et al. (2013) who use normalized difference vegetation index (NDVI) data from the Advanced Very High Resolution Radiometer (AVHRR) satellite to calculate average LAI for the period 1981 – 2010.

2.4 Experimental setup

2.4.1 **Equilibrium pre-industrial simulation**

The equilibrium pre-industrial simulation was initialized from zero biomass and zero fractional coverage for all non-crop PFTs. The fractions of C_3 and C_4 crop PFTs in each grid cell are specified corresponding to year 1850 based on the HYDE 3.1 dataset. The model was then run for 600 years driven by 1901-1925 CRU-NCEP climate data cycled repeatedly. These data do not show any warming trend (Wen et al., 2011) as opposed to the later part of the 20^{th} century. Atmospheric CO_2 concentration was set to 285 ppm corresponding to the pre-industrial 1850 level. This pre-industrial equilibrium simulation yields initial conditions including fractional coverages of PFTs and carbon in all the live and dead pools for the transient 1850-2010 simulation. The 600 years simulation is sufficient for fractional vegetation cover and carbon pools to reach equilibrium.

2.4.2 **Transient historical simulation**

The transient historical simulation is performed for the period 1851-2010 and its carbon pools and fractional coverage of non-crop PFTs are initialized from the equilibrium pre-industrial simulation as mentioned above. The years 1851 to 1900 of this historical simulation are driven

with CRU-NCEP climate data corresponding to the period 1901-1925, cycled twice. For the period 1901-2010 the climate data corresponding to each year are used. Time varying concentrations of atmospheric CO_2 are supplied for the period 1851-2010 based on the values used in the fifth Coupled Modelling Intercomparison Project (CMIP5, http://tntcat.iiasa.ac.at/RcpDb/) which are extended past 2005 to 2010 based on data from the National Oceanic and Atmospheric Administration (ftp://aftp.cmdl.noaa.gov/products/trends/co2/co2_annmean_gl.txt). The annual time-varying fractional coverages of C_3 and C_4 crop PFTs in each grid cell are based on the HYDE 3.1 dataset. The crop fractions in a grid cell are not available for colonization and neither are they subject to disturbance by fire. Competition between PFTs occurs over the remaining non-crop fraction of a grid cell. As total crop fraction in a grid cell changes over time (based on the HYDE 3.1 dataset) the fractional area available for competition also changes.

The simulated results are evaluated against their observation-based counterparts using averaged values over the last 30 years of the simulation corresponding to the period 1981-2010. This is the same and/or very close to the time period for modified WANG06 land cover data set (1981-2010), Beer et al. (2010) GPP (1982-2008), and Zhu et al. (2013) LAI (1981-2010). The only exception is the MODIS-based land cover data which are available for the 2001-2014 period.

3 Results

3.1 Continental scale values of PFT coverage

Figures 2a compares the simulated vegetation areas summed over our North American domain with the WANG06 and MODIS observation-based estimates. In the absence of another measure of uncertainty, we use the range between these two observation-based estimates and assess if simulated areal coverage of a given land cover type lies within or outside this range. The simulated total vegetated area over North America (14.8×10^6 km^2) is very similar to the modified WANG06 (14.4×10^6 km^2) and MODIS derived (14.2×10^6 km^2). At the most basic tree-grass-bare ground level, the simulated areas are closer to the MODIS-based estimates, than to the estimate based on the modified WANG06 data. The simulated area covered by tree PFTs

340 (7.8×10^6 km^2) is 6% lower than the MODIS derived estimate (8.2×10^6 km^2) and 21% lower
341 than WANG06 (9.7×10^6 km^2). The simulated grass coverage (4.7×10^6 km^2) is 35% higher
342 than the MODIS derived estimate (3.5×10^6 km^2). Both simulated and MODIS-based estimates
343 of area covered by grass PFTs are, however, substantially higher than the WANG06 (2.4×10^6
344 km^2) estimate. Averaged over the North American region, the simulated partitioning of land area
345 (excluding cropland area) covered by trees, grasses and bare ground (45%, 27%, 28%) is much
346 closer to the MODIS based data (48%, 20% and 32%) than to the modified WANG06 based data
347 (56%, 14%, 30%).
348
349 Figure 2b shows a comparison of simulated areas of individual PFTs with observation-based
350 estimates. This is a more stringent test of the performance of the competition module of CTEM.
351 The observation-based estimates of areas of all individual PFTs are available for the modified
352 WANG06 dataset. The MODIS based estimates were derived based on the mapping of MODIS'
353 17 land cover types to CTEM PFTs as shown in Table 2, which itself is mostly based on
354 WANG06. In Figure 2b, the observation-based estimates show that needleleaf evergreen (NDL
355 EVG) and broadleaf cold deciduous (BDL DCD CLD) are the dominant tree PFTs across North
356 America and the model is able to reproduce this aspect. The simulated total area of the NDL
357 EVG tree PFT (3.9×10^6 km^2) is 28% less than WANG06 (5.3×10^6 km^2) and 15% less than the
358 MODIS based estimate (4.7×10^6 km^2). The simulated total area of BDL DCD CLD tree PFT (3
359 $\times 10^6$ km^2) is 13% less than WANG06 (3.4×10^6 km^2) and 3% greater than MODIS based ($2.9 \times$
360 10^6 km^2) estimate. Overall, the model is able to capture the areas covered by individual PFTs
361 reasonably well. However, differences remain between observations-based and simulated
362 estimates especially the larger simulated area for C_3 grasses than both observation-based
363 estimates. Reasons for these differences include limitations in the model but also the manner in
364 which remotely-sensed vegetation is categorized into broad-scale vegetation types and then
365 mapped onto CTEM's nine PFTs, as discussed later.
366
367 In both Figures 2a and 2b although simulated areal coverages at the basic tree-grass-bare ground
368 level and for individual PFTs (except for C_3 grasses) are comparable to observation-based

estimates they are outside the range defined by difference of the WANG06 and MODIS based estimates.

Figure 2c shows the time series of simulated areas summed over the domain covered by tree and grass PFTs, the total vegetated area and the remaining bare ground. The specified area covered by crop PFTs, based on the HYDE 3.1 data set, is also shown and first increases over the historical period and then stabilizes and in fact somewhat decreases in association with cropland abandonment over the north-eastern United States. The increase in the crop area results in a decrease in the area covered by tree and grass PFTs up until the time when the crop area stabilizes around 1970. In the model, this causes land use change emissions associated with deforestation. After this time, as vegetation productivity responds to increasing atmospheric CO_2 concentration, the area covered by tree PFTs increases somewhat and colonizes available bare areas and those covered by grass PFTs. This leads to a small reduction in the area covered by grass PFTs as well as bare ground and the associated increase in the total vegetated area.

3.2 Geographical distribution of PFTs

3.2.1 Total vegetated and bare ground fractions

Figures 3 and 4 compare the geographical distribution of simulated total vegetated and bare fractions across North America with the two observation-based estimates derived from the modified WANG06 and MODIS data sets. The two observation-based estimates are also compared amongst themselves. The metrics used are averaged root mean square difference (RMSD) and spatial correlations (R^2).

The observation-based geographical distribution of vegetated fraction in Figure 3 (middle column) shows densely vegetated land over the eastern part of the continent and less vegetation coverage over colder regions in the North and drier regions in the south-central and south-west United States. These broad scale patterns are consistent with the precipitation and temperature climatologies of the region (Figure 1). The model reasonably reproduces the observed vegetation distribution (left panel) with some obvious limitations. Simulated vegetation cover is

underestimated across the arid south-west United States, Great Plains and part of the Canadian Prairies (right panel) due to lower simulated fractional coverage of tree and grass PFTs over these regions (shown in the next section). The model overestimates vegetation coverage in Northern Canada because of higher simulated grass cover in the Arctic as discussed below in more detail. The spatial correlation and RMSD when comparing simulated vegetated fraction to both observation-based estimates are 0.79 and around 18%, respectively. The spatial correlation and RMSD between the two observation-based estimates themselves are 0.86 and around 14%, respectively.

The simulated and observation-based bare ground fractions across North America are compared in Figure 4. The observation-based estimates show that bare ground fraction is higher in Arctic Canada and Alaska where, of course, cold temperatures limit vegetation growth and in the south-west United States, Great Plains and the Prairies where low rainfall limits vegetation growth (Figure 1). The biases in simulated bare ground fraction mirror those in the simulated vegetated fraction but in an opposite manner. The model underestimates bare ground fraction across Arctic Canada due to higher simulated grass cover as discussed in the next section. The model overestimates the bare ground fraction generally across the arid and semi-arid south-west United States, Great Plains and the Prairies. The spatial correlations and RMSDs when comparing simulated bare ground fraction to both observation-based estimates, and when comparing the two observation-based data sets amongst themselves are the same as those for the total vegetation fraction in Figure 3.

3.2.2 **Tree and grass cover**

Figure 5 compares the simulated tree cover with the two observation-based estimates. The model reasonably reproduces the broad scale patterns including the Canadian boreal forest and the temperate forests across the southeastern United States. However, the model simulates lower tree cover across the western part of the continent compared to both observation-based estimates particularly over the southwestern United States which is characterized by arid climate (Figure 1). The observation-based estimates do not particularly well agree over this region either. The MODIS derived estimate suggests around 25% tree cover in the southwestern United States

while the WANG06 derived estimate suggests a tree cover of around 60% over a large area in the region. The spatial correlation and RMSD when comparing simulated tree cover to both observation-based estimates are around 0.68 and around 17%, respectively. The spatial correlation and RMSD between the two observation-based estimates themselves are 0.75 and around 15%, respectively. Possible reasons for differences between simulated and observation-based estimates are discussed in detail in the discussion section and include the fact that the CLASS-CTEM framework does not currently represent shrubs and there are limitations in the observation-based data sets themselves. Shrubs are more prevalent in arid and semi-arid regions where they are better suited to grow compared to both trees and grasses.

Figure 6 compares the geographical distribution of the simulated grass cover with the two observation-based estimates. The broad geographical distribution of simulated grass cover compares well with the two observation-based estimates with the notable exception of the Arctic region including Alaska and northern Canada, where the model overestimates grass cover. This overestimation of grass cover in the Arctic region is also the reason for the overestimation of total vegetation fraction and the underestimation of bare fraction that was seen earlier in Figures 3 and 4 respectively.

As shown in Figure 6, the spatial correlation and RMSD when comparing simulated grass cover to both observation-based estimates lie between 0.33 and 0.38 and between around 15-17%, respectively. The spatial correlation and RMSD between the two observation-based estimates themselves are 0.54 and around 9%, respectively. The two observation-based estimates disagree most markedly over the western half of the United States where the MODIS derived estimates of grass cover are higher.

3.2.3 **Needleleaf evergreen and broadleaf cold deciduous trees**

Figures 7a and 7b compare the geographical distribution of NDL EVG and BDL DCD CLD trees, respectively, with their observation-based estimates. These two are the primary tree PFTs which exist in the North American domain considered here.

In Figure 7a, the overall simulated coverage of NDL EVG trees is lower than both observation-based estimates as was also seen in Figure 2b. The simulated values are primarily lower in western Canada and over a large area in the western United States according to estimates based on the modified WANG06 data set. This is also the case along the wide swath of the Canadian boreal forest. The model overestimates the coverage of NDL EVG trees in the eastern United States. The spatial correlation and RMSD when comparing simulated coverage of NDL EVG trees to both observation-based estimates lie between 0.36 and 0.40 and between around 16-17%, respectively. The spatial correlation and RMSD between the two observation-based estimates themselves are 0.52 and around 16%, respectively.

The geographical distribution of BDL DCD CLD trees is compared with its observation-based estimates in Figure 7b. Although the simulated domain summed area of BDL DCD CLD trees (3×10^6 km^2) is comparable to estimates based on the modified WANG06 (3.4×10^6 km^2) and MODIS (2.9×10^6 km^2) data sets, there are two primary limitations in its simulated geographical distribution. First, the simulated values are generally overestimated in Canadian boreal forests and underestimated in the eastern United States. Second, the model simulates near zero coverage in the arid south-western United States. The spatial correlation and RMSD when comparing simulated coverage of BDL DCD CLD trees to both observation-based estimates are around 0.3 and around 12%, respectively. The spatial correlation and RMSD between the two observation-based estimates themselves are 0.60 and around 8%, respectively.

3.2.4 **C_3 and C_4 grasses**

Figures 8a and 8b compare the simulated geographical distribution of C_3 and C_4 grasses with observation-based estimates.

In Figure 8a, the most obvious limitation of the model is its excessive simulated grass coverage in Alaska and in Arctic Canada. Other than this, the model reproduces the broad geographical distribution of C_3 grasses including the Great Plains of United States and the Canadian Prairies, where a large extent of grasslands is observed. The overestimated grass coverage at high latitudes leads to a total simulated C_3 grass area (4.4×10^6 km^2) that is higher than estimates

493 based on the modified WANG06 (1.9×10^6 km^2) and MODIS (2.8×10^6 km^2) data sets. The
494 spatial correlation and RMSD when comparing simulated coverage of C_3 grasses to both
495 observation-based estimates lie between 0.34-0.38 and between around 15-17%, respectively.
496 The spatial correlation and RMSD between the two observation-based estimates themselves are
497 0.54 and around 12%, respectively.
498
499 Figure 8b shows the distribution of C_4 grasses which mostly occur in the tropics and do not
500 occupy large areas in North America (as was also seen in Figure 2b). The modelled geographical
501 distribution of C_4 grasses is larger than observation-based estimates but the absolute fractions
502 remain small so that the simulated area covered over the whole domain (0.35×10^6 km^2) is
503 actually smaller than estimates based on the modified WANG06 (0.45×10^6 km^2) and MODIS
504 (0.7×10^6 km^2) data sets. The spatial correlation and RMSD when comparing simulated
505 coverage of C_4 grasses to both observation-based estimates lie between 0.12-0.16 and between
506 around 3-5%, respectively. The spatial correlation and RMSD between the two observation-
507 based estimates themselves are 0.62 and around 5%, respectively.
508
509 We do not compare the spatial distribution of broadleaf evergreen (BDL EVG) and broadleaf
510 drought deciduous (BDL DCD DRY) trees with the two observation-based estimates for three
511 reasons: 1) the geographical distribution of these PFTs is limited to a small total area in our
512 domain, 2) the geographical distribution of the BDL EVG tree PFT based on observations cannot
513 be directly compared to simulated values because, when mapping land cover types to CTEM
514 PFTs in WANG06, evergreen shrubs (which exist much farther north than 30 °N) are assigned to
515 the BDL EVG tree PFT, and 3) the geographical distribution of the BDL DCD DRY tree PFT in
516 the observation-based data sets is based on the arbitrary latitudinal thresholds of 24 °N and 34 °N
517 as mentioned earlier.
518
519 **3.3 LAI and GPP**
520
521 Figure 9 compares the geographical distribution of simulated LAI and GPP with observation-
522 based estimates for the present day. In Figure 9a, the simulated geographical distribution of LAI
523 compares well with the observation-based estimates. The spatial correlation and RMSD between

simulated and observation-based estimates are 0.74 and 0.81 m^2/m^2, respectively. The domain averaged simulated LAI of 2.5 m^2/m^2 is higher than the observation-based estimate of 2.1 m^2/m^2. The model captures the broad geographical patterns with higher LAI over the boreal forest region in Canada and also in the eastern United States similar to observations. However, some differences remain particularly over the drier southwest United States where the model simulates bare ground with negligible LAI but observations suggest a small LAI of around 1 m^2/m^2. In contrast, the model slightly overestimates LAI over northern and Arctic Canada where it simulates a higher fractional coverage of C_3 grasses, as seen earlier.

Consistent with the geographical distribution of LAI, the simulated GPP is overestimated in the eastern United States and the Canadian boreal forest (Figure 9b). The broad geographical distribution of GPP, similar to LAI, is consistent with the observation-based estimates. The spatial correlation and RMSD between simulated and observation-based estimates are 0.78 and 225 gC/m^2.year, respectively. The domain averaged simulated GPP of 737 gC/m^2.year is higher than the observation-based estimate of 628 gC/m^2.year. As with LAI, the simulated GPP is lower than observations over the drier southwest region of the United States where the model simulates more bare ground than observation-based estimates, and the model overestimates GPP over the northern and Arctic Canada.

Figure 10 shows the time series of annual domain averaged GPP, LAI, net primary productivity (NPP) and domain summed net biome productivity (NBP). The NBP term is essentially the net atmosphere-land CO_2 flux which is the result of all terrestrial ecosystem processes including photosynthesis, autotrophic and heterotrophic respiration, fire and land use change. NBP values of zero indicate that the system is in equilibrium such that carbon gained by photosynthesis is equal to carbon lost by respiration and other processes. Simulated GPP, LAI and NPP all show an increase over the 20^{th} century due to the increase in atmospheric CO_2 concentration and the associated change in climate. The increase in CO_2 drives the increase in GPP and subsequently in NPP and LAI through the CO_2 fertilization effect. The net result of this gradually increasing NPP is that the terrestrial ecosystems become a sink of carbon and this is seen in the resulting positive values of NBP. The simulated sink over the North American domain for the periods 1990-2000 and 2000-2010 is around 0.4 and 0.5 Pg C/year, respectively. Crevoisier et al. (2010) compare

555 the carbon sink over the North American region from five studies (their Table 1) for time periods
556 in the 1990s and 2000s. These reported sinks vary from 0.81±0.72 to 1.26±0.23 Pg C/year for the
557 period 1992-1996, 0.58 Pg C/yr for the period 2001-2006 and Crevoisier et al. (2010) themselves
558 estimate a value of 0.51 ± 0.41 Pg C/yr for the period 2004-2006. The sinks simulated by
559 CLASS-CTEM over the 1990s and 2000s are broadly consistent with these estimates.
560
561 ### 3.4 Added value of finer spatial resolution
562
563 Figure 11 assesses the added value of running the model and performing competition between
564 PFTs at the 1° spatial resolution used in this study compared to the 3.75° resolution used in
565 Melton and Arora (2016) study which evaluated the performance of CLASS-CTEM's
566 competition module at the global scale. For Figure 11, the Melton and Arora (2016) results were
567 extracted for the North American domain used in this study and observation-based estimates of
568 fractional coverage of tree, grass and total vegetation from the modified WANG06 land cover
569 product were re-gridded to the 3.75° resolution. The resulting spatial correlations and RMSDs
570 between the simulated and the WANG06 estimates for fractional coverage of tree, grass and total
571 vegetation, at the two spatial resolutions, are summarized in Figure 11. When compared to the
572 modified WANG06 data the RMSDs are somewhat lower (Figure 11a), and spatial correlations
573 (Figure 11b) are slightly higher for model's implementation at 3.75° resolution, compared to
574 model's implementation at 1° resolution. This indicates that the model's performance is slightly
575 better at the coarser 3.75° resolution. Recall that competition between PFTs occurs over the non-
576 crop fraction of each grid cell. For this reason, we do not perform this analysis for MODIS based
577 land cover product because the crop areas that are specified in the model are exactly same as
578 those in the modified WANG06 land cover product making comparison of simulated and
579 observation-based fractional coverages of PFTs more consistent for the modified WANG06 land
580 cover product.
581
582 ## 4 Discussion
583
584 Competition between PFTs, that determines their fractional coverage, is one of the several
585 processes that the CLASS-CTEM modelling framework simulates. Other than competition

between PFTs, terrestrial ecosystem processes of photosynthesis, autotrophic and heterotrophic respiration, allocation of carbon from leaves to stem and root components, dynamic leaf phenology, fire, and land use change are also modelled. These aspects of the model have been evaluated at point (Arora, 2003; Arora and Boer, 2005; Melton et al., 2015), regional (Garnaud et al., 2015; Peng et al., 2014; Arora et al., 2016) and global (Arora and Boer, 2010; Melton and Arora, 2014; Melton and Arora, 2016) scales. A typical model evaluation exercise at the global scale compares model simulated geographical and latitudinal distribution of GPP, vegetation biomass, and soil carbon with their respective observation-based estimates such as those from Beer et al. (2010), Ruesch and Holly (2008) and Harmonized World Soil Database (FAO/IIASA/ISRIC/ISS-CAS/JRC, 2012). Model evaluation exercises help in identifying model limitations but also yield opportunities to improve model performance by tuning model parameters. CLASS-CTEM model also participated in the 2016 TRENDY intercomparison of terrestrial ecosystem models whose results contributed to the global carbon project (Le Quéré et al., 2016). The competition module of the CLASS-CTEM modelling framework has been previously evaluated at point scales (Arora and Boer, 2006; Shrestha et al., 2016). In addition to assessing fractional coverage at which PFTs equilibrate, these point scale evaluations also assess the time the PFTs take to reach their equilibrium fractional coverages against empirical data and if the succession patterns are realistically simulated (e.g. grasses should colonize a given area before trees invade the area covered by grasses). This manuscript focusses on evaluation of the competition module of the CLASS-CTEM modelling framework at a regional scale.

Dynamically simulated fractional coverages of PFTs adds another degree of freedom to a model compared to the case where the fractional coverages of its PFTs are specified. This is a more stringent test of a model's performance. Errors in the simulated geographical distribution of PFTs will, of course, lead to corresponding errors in the geographical distribution of primary terrestrial ecosystem carbon pools and fluxes. Yet, the CLASS-CTEM model is broadly able to reproduce the geographical distributions of GPP and LAI. Limitations, of course, remain. In particular, the simulated LAI and GPP are high in Alaska and in northern and Arctic Canada, and these variables are lower than their observation-based estimates in arid regions of the western United States. The simulated fractional vegetation coverage reflects these patterns.

It is difficult to conclusively determine whether these model limitations are due to the limitations in the biogeochemistry parameterizations of the model for its existing PFTs or the simple structural limitation that the model does not represent shrub, moss and lichen PFTs. Shrubs are adapted to grow in arid and semi-arid regions, whether in cold or hot climates (where neither grasses nor trees are able to grow) and their representation in the model would likely help to increase the fractional vegetation cover in arid regions including those in the western United States. At high latitudes grass growth is inhibited by mosses and lichens which flourish in cold and damp conditions. A representation of moss and lichen PFTs and improved representation of permafrost in the model would likely help to decrease simulated grass coverage in Arctic regions. In the current version of the CLASS-CTEM model bioclimatic limits are used only for tree PFTs to ensure that these PFTs do not venture outside their pre-determined bioclimatic zones. In the model, bioclimatic limits are not used for grasses and their geographical distribution is entirely the result of plant physiological processes and their competitive interactions with the tree PFTs and amongst themselves. Since, in the Arctic region, grasses do not face competition from tree PFTs, and moss and lichen PFTs are not represented in the model, they are free to increase their expanse – climate permitting, of course. Another possible reason for higher than observed grass coverage in the Arctic region is that in the current implementation of CLASS only three permeable soil layers with maximum thicknesses of 0.1, 0.25 and 3.75 m are represented and a boundary condition of zero heat flux is assumed across the bottommost layer. This simple representation does not allow to model permafrost realistically. Permafrost is more realistically modelled with multiple permeable and impermeable (extending into the bed rock) layers that go sufficiently deep (> 30 m at least) to capture the slow evolution of soil temperatures in response to climate warming (Teufel et al., 2017). The current set up of three layers that go only 4.1 m deep produces soil temperatures that are warmer than in the set up when permeable and impermeable layers are sufficiently deep and produces permafrost extent that is lower than observation-based estimates (Koven et al., 2013). It is likely that warmly biased soil temperatures in the current set up contribute to promote grass growth and allow it to cover a larger area in the Arctic region than would be the case when permafrost is more realistically modelled.

The lower than observed fractional vegetation cover in the arid and semi-arid regions of the western United States, however, may not solely be due to model limitations alone. Here, we argue that the manner in which remotely sensed land cover types are mapped to CTEM PFTs, and the errors in calculating bare ground fraction in remotely sensed products also contribute to mismatch between modelled and observation-based values of fractional vegetation cover. We illustrate this by comparing the functional relationship between LAI and total vegetation cover. Figure 12a shows this relationship for model simulated values. As expected, as LAI increases so does the total vegetation cover. The relationship between these two variables is fairly tight in the model and the green line is an exponential fit. The red dots in the figure correspond to grid cells that lie in the region identified in the inset in Figure 12d and broadly correspond to the western half of the United States. Figures 12b and 12c show the same relationship but between the observation-based estimate of LAI from Zhu et al. (2013) (as mentioned in Section 2.3.2) and the total vegetation cover based on the WANG06 and MODIS derived land cover data sets, respectively. The blue and magenta lines in Figures 12b and 12c are the corresponding exponential fits. When compared with Figure 12a, Figures 12b and 12c show much more scatter around the fitted curves, and the overall relationship appears to break down for the red dots corresponding to the grid cells in the western United States. A careful look at the red dots in Figures 12b and 12c shows that the observation-based vegetation cover in the Western United States for a large fraction of grid cells is around 60% regardless of the observation-based LAI which ranges between 0.1 and 1.5 m^2/m^2. Clearly, it is physically unrealistic to achieve fractional vegetation coverage of 60% below LAI values of 0.6 m^2/m^2 (the m^2/m^2 unit implies m^2 of leaf area per m^2 of ground area) and this indicates that the fractional vegetation cover in this region is likely overestimated in both observation-based data sets.

There are at least two ways in which errors in total vegetation cover can occur. The first relates to the method by which the fractional vegetation cover is calculated for the land cover types in the original remotely sensed land cover products: that is, for the 22 land cover types in the GLC2000 data set upon which the WANG06 data are based and the 17 land cover types in the MODIS data set. An example of such an error for arid regions is illustrated by Lawley et al. (2014) who suggest that the MODIS soil fractional cover product, at least in its present form, is unsuited to monitoring sparsely vegetated arid landscapes and generally unable to separate soil

678 from vegetation in situations where normalized difference vegetation index (NDVI) is low. The
679 second way in which errors are introduced is through the mapping of the remotely sensed land
680 cover types to the CTEM PFTs following Table 2 of WANG06 for the GLC2000 land cover
681 types, and following Table 2 in this manuscript for the MODIS land cover types. This mapping
682 is based on available information in the literature but is also based on expert judgement which
683 introduces subjectiveness. For instance, it is debatable what fraction of the "open shrublands"
684 MODIS land cover type, which exists over much of the arid southwestern United States, is in
685 fact bare ground. In Table 2, we have allocated a fraction of 0.4 of "open shrublands" to bare
686 ground following WANG06. Had WANG06 allocated a higher value than this to bare ground,
687 our simulated values would have compared better with the observation-based values of bare
688 ground fraction over arid regions. Nevertheless this would not have changed the relationship, or
689 rather the lack thereof, between the observation-based estimates of LAI and the total vegetation
690 cover in the western half of the United States seen in Figures 12b and 12c.
691
692 Both model and observation-based results are also affected by a common limitation associated
693 with peatlands which exists in the Hudson Bay lowlands region. Both the GLC2000 data set,
694 upon which the modified WANG06 land cover product is based, and the MODIS land cover data
695 do not represent peatland vegetation. In these data sets the peatland vegetation is classified either
696 as grasses, shrubs or trees. The model also does not represent peatlands and as a result the model
697 grows trees and grasses in regions where peatlands exists. Work is under way to incorporate a
698 peatland model developed for CLASS-CTEM (Wu et al., 2016) into our modelling framework.
699
700 The simulated areas covered by the primary two tree PFTs (NDL EVG and BDL DCD COLD)
701 have their weaknesses but large differences also exist between the two observation-based
702 estimates especially for the NDL EVG PFT. Modelling competition between two tree PFTs is
703 much more difficult than between trees and grasses. In the latter case trees are always considered
704 superior to grasses, but in the case of competition between two tree PFTs the superiority is based
705 on parameterized colonization rates which depend on simulated NPP. Based on comparisons
706 with observation-based estimates, the main limitation in model results here is that the model
707 overestimates the coverage of NDL EVG trees, and underestimates the coverage of BDL DCD
708 COLD trees in the eastern United States, while the opposite is true in western Canada. The

model, of course, does not represent individual species, while in the real world competition occurs at the species level that is modulated by soils and nutrient availability. An example that illustrates this limitation of the model is the Jack pine tree species which occupies ecological niche of nutrient poor soils in Boreal Canada (e.g. see Ste-Marie et al., 2007). The coupling of carbon and nutrient cycles is currently not represented in CLASS-CTEM and optimizing model parameters for hundreds of species is currently extremely difficult given limited available data at the species level. Most likely before the model is applied at the species level, as a first step, the number of PFTs represented in the model should be increased. An example of how additional PFTs in the CLASS-CTEM framework can lead to improved model performance is illustrated by Peng et al. (2014). This application of the model shows how sub-dividing the NDL EVG PFT into coastal and interior types for the province of British Columbia in Canada leads to improvement in simulated LAI and GPP. A recent attempt to explicitly represent physiological process in a model to simulate competition between needleleaf and broadleaf cold deciduous trees at a regional scale is illustrated in (Fisher et al., 2015) who incorporated the concepts from the Ecosystem Demographics (ED) model into the community land model – dynamic vegetation model (CLM-DGVM). Their results provide some interesting insights; however, validation of this approach at the global scale over a wide range of PFTs remains challenging.

Finally, one of the objectives of this study was to evaluate if resolving climate niches by performing CLASS-CTEM simulation at a finer resolution of 1° in this study allowed improved simulation of geographical distribution of PFTs than in the Melton and Arora (2016) study that evaluated the competition module of the CLASS-CTEM model at 3.75° spatial resolution at the global scale. Figure 11 addresses this objective and shows that while the spatial correlations and RMSDs between the simulated and the modified WANG06 land cover product for fractional coverage of tree, grass and total vegetation are fairly similar for the model outputs at 1° and 3.75° resolutions, these metrics are somewhat better for model's application at the coarser 3.75° resolution. One possible reason for the slightly worse model performance at the finer resolution is that while climate niches are resolved better at the finer resolution the model does not have the additional differentiation in PFTs (the number of model PFTs is still nine) that is required to gain benefit from the resolved climate niches. In addition, comparing Melton and Arora (2016) results over North America with ones obtained here we note that the primary model limitations remain

unchanged in the application of the model at both spatial resolutions. These include lower simulated fractional vegetation coverage in the arid south-west North American region and higher in the Arctic region (due to higher grass coverage). In addition, in both applications of the model the differences in simulated geographical distribution of NDL EVG and BDL DCD CLD PFTs, compared to the WANG06 land cover data, are also similar. Model differences, compared to the WANG06 data, therefore remain more or less similar in the application of the model at both spatial resolutions. These results are, however, based on offline applications of the CLASS-CTEM model where it is driven by reanalysis data. In a fully-coupled simulation where CLASS-CTEM is coupled to an atmospheric model it is possible that model performance at low spatial resolution is different from its performance at high spatial resolution

The comparison between observation-based and simulated fractional coverages is the most robust at the basic tree-grass-bare ground level. The subjectiveness introduced in the process of mapping remotely sensed land cover types to the PFTs represented in a model, as mentioned above, makes the comparison of simulated and observation-based fractional coverages for individual PFTs less robust. Nevertheless, comparisons with observations allow useful insights into model limitations as we have seen here.

5 Summary and conclusions

This study evaluates the CLASS-CTEM simulated fractional coverages of PFTs, when driven with observed meteorological forcing, against the observation-based estimates from MODIS and the modified WANG06 data sets over the North American region. In the past, performance of the competition module of the CLASS-CTEM modelling framework has been assessed at global scale, at a coarse spatial resolution of 3.75° (Melton and Arora, 2016), as well as at point scale, for a range of locations across the globe (Shrestha et al., 2016). Our objective here was to assess the performance of the CLASS-CTEM competition module at a higher spatial resolution of 1° over North America. To achieve this objective we compared simulated present day geographical distributions of fractional coverages of PFTs, but also LAI and GPP with their observation-based estimates.

The CLASS-CTEM modelling framework is generally able to reproduce the dominant features of the geographic distribution of PFT coverage, and LAI and GPP over the North American region. After 1960, the model simulates increasing GPP and LAI in response to changing climate as well as increased atmospheric CO_2 concentrations and the resulting sink for the 1990s and 2000s is broadly consistent with other estimates.

The simulated geographical distribution of PFTs, when compared to observation-based estimates, show two primary limitations which are excessive grass cover in the Arctic region and low vegetation cover in the arid western United States, although for the latter the observation-based estimates themselves may have their own weaknesses. There are three main factors in the CLASS-CTEM modelling framework that may have contributed to these differences: 1) the absence of a shrub PFT, which we believe is the reason for low simulated vegetation coverage in the arid to semi-arid western United States, 2) the absence of moss and lichen PFTs that may inhibit the establishment of grasses, and 3) probably a lack of sensitivity of C_3 grasses to high latitude climate and an inadequate representation of permafrost. Future model developments will focus on these aspects with a view to improving model performance.

References:

Anav, A., Friedlingstein, P., Kidston, M., Bopp, L., Ciais, P., Cox, P., Jones, C., Jung, M., Myneni, R., and Zhu, Z.: Evaluating the land and ocean components of the global carbon cycle in the CMIP5 earth system models, J. Climate, 26, 6801-6843, doi:10.1175/JCLI-D-12-00417.1, 2013.

Arora, V. K.: Land surface modelling in general circulation models: a hydrological perspective, PhD Thesis, University of Melbourne, Australia, 1997.

Arora, V.K.: Simulating energy and carbon fluxes using coupled land surface and terrestrial ecosystem models, Agricultural and Forest Meteorology, 118(1-2), 21-47, 2003.

Arora, V. K. and Boer, G. J.: A representation of variable root distribution in dynamic vegetation models, Earth Interactions, 7, 1-19, 2003.

Arora, V. K. and Boer, G. J.: A parameterization of leaf phenology for the terrestrial ecosystem component of climate models, Glob. Change Biol., 11, 39-59, 2005.

Arora, V. K. and Boer, G. J.: Simulating Competition and Coexistence between Plant Functional Types in a Dynamic Vegetation Model, Earth Interactions, 10, 1-29, 2006.

Arora, V.K. and G.J. Boer: Uncertainties in the 20th century carbon budget associated with land use change, Global Change Biology, 16(12), 3327–3348, 2010.

Arora, V. K., Boer, G. J., and Friedlingstein, P. E. A.: Carbon-concentration and carbon-climate feedbacks in CMIP5 earth system models, J. Climate, 26, 5289-5314, 2013.

Arora, V. K., Y. Peng, W. A. Kurz, J. C. Fyfe, B. Hawkins, and A. T. Werner: Potential near-future carbon uptake overcomes losses from a large insect outbreak in British Columbia, Canada, Geophys. Res. Lett., 43, doi:10.1002/2015GL067532, 2016.

Beer, C., Reichstein, M., Tomelleri, E., Ciais, P., Jung, M., Carvalhais, N., Rodenbeck, C., Arain, M. A., Baldocchih, D., Bonan, G. B., Bondeau, A., Cescatti, A., Lasslop, G., Lindroth, A., Lomas, M., Luyssaert, S., Margolis, H., Oleson, K. W., Roupsard, O., Veenendaal, E., Vivoy, N., Williams, C., Woodward, F. I., and Papale, D.: Terrestrial gross carbon dioxide uptake: global distribution and covariation with climate, Science, 329, 834-838, doi:10.1126/science.1184984, 2010.

Bonan, G. B.: Forests and climate change: Forcings, feedbacks, and the climate benefits of forests, Science, 320, 1444-1449, doi:10.1126/science.1155121, 2008.

Box, E. O.: Plant functional types and climate at the global scale, J. Veg. Sci., 7, 309-320, doi:10.2307/3236274, 1996.

Brentnall, S. J., Beerling, D. J., Osborne, C. P., Harland, M., Francis, J. E., Valdes, P. J., and Wittig, V. E.: Climatic and ecological determinants of leaf lifespan in polar forests of the high CO2 Cretaceous 'greenhouse' world, Glob. Change Biol., 11, 2177-2195, 2005.

Broxton, P., X. Zeng, D. Sulla-Menashe, and P. Troch, 2014: A Global Land Cover Climatology Using MODIS Data. J. Appl. Meteor. Climatol., 53, 1593–1605, doi: 10.1175/JAMC-D-13-0270.1.

Cox, P. 2001: Description of the "TRIFFID" Dynamic Global Vegetation Model. Tech. Note 24.

Cramer, W., Bondeau, A., Woodward, F. I., Prentice, I. C., Betts, R. A., Brovkin, V., Cox, P. M., Fisher, V., Falloon, P. D., Foley, J., Friend, A. D., Kucharik, C., Lomas, M. R., Ramankutty, N., Sitch, S., Smith, B., White, A., and Molling-Young, C.: Global response of terrestrial ecosystem structure and function to CO2 and climate change: results from six dynamic global vegetation models, Global Change Biology, 7, 357-373, 2001.

Crevoisier, C., Sweeney, C., Gloor, M., Sarmiento, J. L., and Tans, P. P.: Regional US carbon sinks from the three-dimensional atmospheric CO2 sampling, PANAS, 107, 18348-18353, DOI: 10.1073/pnas.0900062107, 2010.

Dai, Y., Zeng, X., Dickinson, R. E., and Coauthors: Common Land Model (CLM), Technical documentation and user's guide. [Available online at [http://climate.eas.gatech.edu/dai/clmdoc.pdf.], 2001.

FAO/IIASA/ISRIC/ISS-CAS/JRC: Harmonized World Soil Database (version 1.2), available at: http://www.fao.org/soils-portal/soil-survey/soil-maps-and-databases/harmonized-world-soil-database-v12/en/ (last access: 20 January 2016), 2012.

Fisher, R. A., Muszala, S., Verteinstein, M., Lawrence, P., Xu, C., Mcdowell, N. G., Knox, R. G., Koven, C., Holm, J., Rogers, B. M., Spessa, A., Lawrence, D., and Bonan, G.: Taking off the training wheels: the properties of a dynamic vegetation model without climate envelopes, CLM4.5(ED), Geosci. Model Dev., 8, 3593-3619, doi:10.5194/gmd-8-3593-2015, 2015.

Friedl, M., Strahler, A., Schaaf, C., Hodges, J. C. F., and Salomon, J., 2013:.: Binary MODIS MOD12C1 0.25 Degree Land Cover Climate Modeler Grid. Available at [http://duckwater.bu.edu/lc/] from the Department of Geography, Boston University, Boston, Massachusetts, USA., 2013.

Friedlingstein, P., Cox, P., Betts, R., Bopp, L., Von Bloh, W., Brovkin, V., Cadule, P., Doney, S., Eby, M., Fung, I., Bala, G., John, J., Jones, C., Joos, F., Kato, T., Kawamiya, M., Knorr, W., Lindsay, K., Matthews, H. D., Raddatz, T., Rayner, P., Reick, C., Roeckner, E., Schnitzler, K.-G., Schnur, R., Strassmann, K., Weaver, A. J., Yoshikawa, C., and Zeng, N.: Climate–carbon cycle feedback analysis: Results from the C4MIP model intercomparison, J. Climate, 19, 3337-3353, 2006.

Friend, A. D., Chard, Lucht, W., Rademacher, T., Keribin, R., Betts, R., Cadule, P., Ciais, P., Clark, D. B., Dankers, R., Falloon, P. D., Ito, A., Kahana, R., Kleidon, A., Lomas, M. R., Nishina, K., Ostberg, S., Pavlick, R., Peylin, P., Schaphoff, S., Vuichard, N., Warszawski, L., Wiltshire, A., and Woodward, F. I.: Carbon residence time dominates uncertainty in terrestrial vegetation response to future climate and atmospheric CO2, Proc. Natl. Acad. Sci. USA, 111, 3280-3285, 2013.

Garnaud, C., Sushama, L., and Verseghy, D.: Impact of interactive vegetation phenology on the Canadian RCM simulated climate over North America, Climate Dynamics, 45, 1471-1492, doi:10.1007/s00382-014-2397-9, 2015.

Gobron, N., Belward, A., and Knorr, W.: Monitoring biosphere vegetation 1998-2009, Geophys. Res. Lett., 37, L15402, 2010.

Hurtt, G. C., Chini, L. P., Frolking, S., Betts, R. A., Feddema, J., Fischer, G., Fisk, J. P., Hibbard, K., Houghton, R. A., Janetos, A., Jones, C. D., Kindermann, G., Kinoshita, T., Klein Goldewijk, K., Riahi, K., Shevliakova, E., Smith, S., Stehfest, E., Thomson, A., Thornton, P., Van Vuuren, D. P., and Wang, Y. P.: Harmonization of land-use scenarios for the period 1500-2100: 600 years of global gridded annual land-use transitions, wood harvest, and resulting secondary lands, Climate Change, 109, 117-161, 2011.

Kramer, P. J. and Kozlowski, T. T., 1979:.: Physiology of woody plants. Academic press, 1979.

Koven, C. D., Riley, W. J. and Stern, A.: Analysis of Permafrost Thermal Dynamics and Response to Climate Change in the CMIP5 Earth System Models, J. Clim., 26(6), 1877–1900, 2013.

Lawley, E. F., Lewis, M. M., and Ostendorf, B.: Evaluating MODIS soil fractional cover for arid regions, using albedo from high-spatial resolution satellite imagery, Int. J. Remote Sens., 35, 2028-2046, 2014.

Le Quéré, C., Andrew, R. M., Canadell, J. G., Sitch, S., Korsbakken, J. I., Peters, G. P., Manning, A. C., Boden, T. A., Tans, P. P., Houghton, R. A., Keeling, R. F., Alin, S., Andrews, O. D., Anthoni, P., Barbero, L., Bopp, L., Chevallier, F., Chini, L. P., Ciais, P., Currie, K., Delire, C., Doney, S. C., Friedlingstein, P., Gkritzalis, T., Harris, I., Hauck, J., Haverd, V., Hoppema, M., Klein Goldewijk, K., Jain, A. K., Kato, E., Körtzinger, A., Landschützer, P., Lefèvre, N., Lenton, A., Lienert, S., Lombardozzi, D., Melton, J. R., Metzl, N., Millero, F., Monteiro, P. M. S., Munro, D. R., Nabel, J. E. M. S., Nakaoka, S.-I., O'Brien, K., Olsen, A., Omar, A. M., Ono, T., Pierrot, D., Poulter, B., Rödenbeck, C., Salisbury, J., Schuster, U., Schwinger, J., Séférian, R., Skjelvan, I., Stocker, B. D., Sutton, A. J., Takahashi, T., Tian, H., Tilbrook, B., van der Laan-Luijkx, I. T., van der Werf, G. R., Viovy, N., Walker, A. P., Wiltshire, A. J., and Zaehle, S.: Global Carbon Budget 2016, Earth Syst. Sci. Data, 8, 605-649, doi:10.5194/essd-8-605-2016, 2016.

Melton, J. R. and Arora, V. K.: Competition between plant functional types in the Canadian Terrestrial Ecosystem Model (CTEM) v. 2.0, Geosci. Model Dev., 9, 323-361, 2016.

Melton, J. R. and Arora, V. K. (2014) Sub-grid scale representation of vegetation in global land surface schemes: Implications for estimation of the terrestrial carbon sink, Biogeosciences, 11(4), 1021-1036.

Melton, J. R., Shrestha, R. K., and Arora, V. K.: The influence of soils on heterotrophic respiration exerts a strong control on net ecosystem productivity in seasonally dry Amazonian forests, Biogeosciences, 12, 1151-1168, doi:10.5194/bg-12-1151-2015, 2015.

Peng, Y., Arora, V. K., Kurz, W. A., Hember, R. A., Hawkins, B. J., Fyfe, J. C., and Werner, A. T.: Climate and atmospheric drivers of historical terrestrial carbon uptake in the province of British Columbia, Canada, Biogeosciences, 11, 635-649, doi:10.5194/bg-11-635-2014, 2014.

Pielke, R. A., Avissar, R., Raupach, M., Dolman, A. J., Zeng, X., and Denning, S.: Interactions between the atmosphere and terrestrial ecosystem: influence on weather and climate, Global Change Biology, 4, 461-475, 1998.

Ramankutty, N. and Foley, J. A.: Estimating historical changes in global land cover: Croplands from 1700 to 1992, Global Biogeochem. Cycles, 13, 997-1027, 1999.

Ran, L., Pleim, J., Gilliam, R., Binkowski, F. S., Hogrefe, C., and Band, L.: Improved meteorology from an updated WRF/CMAQ modeling system with MODIS vegetation and albedo, J. Geophys. Res. Atmos., 121, 2393-2415, doi:10.1002/2015JD024406, 2016.

Ruesch, A. and Holly, K.: New IPCC Tier-1 Global Biomass Carbon Map For the Year 2000, available at: ftp://cdiac.ornl.gov/ pub/global_carbon/ (last access: 5 July 2013), Carbon Dioxide Information Analysis Center http://cdiac.ornl.gov (last access: 5 July 2013), Oak Ridge National Laboratory, Oak Ridge, Tennessee, 2008.

Ritchie, T. C. and Macdonald, G. M.: The patterns of post-glacial spread of White Spruce, J. Biogeogr., 13, 527-540, 1986.

Shrestha, R. K., Arora, V. K., and Melton, J. R.: The sensitivity of simulated competition between different plant functional types to sub-grid-scale representation of vegetation in a land surface model, J. Geophys. Res. Biogeosci., 121, doi:10.1002/2015JG003234, 2016.

Siemann, E. and Rogers, W. E.: Changes in light and nitrogen availability under pioneer trees may indirectly facilitate tree invasion of grasslands, J. Ecology, 91, 923-931, 2003.

Sitch, S., Smith, B., Prentice, I. C., Arneth, A., Bondeau, A., Cramer, W., Kaplan, J. O., Lucht, W., Sykes, M. T., Thonicke, K., and Venevsky, S.: Evaluation of ecosystem dynamics, plant geography and terrestrial carbon cycling in the LPJ dynamic global vegetation model, Glob. Change Biol., 9, 161-185, 2003.

Ste-Marie, C., Paré D, and Gagnon, D. : The contrasting effects of Aspen and Jack Pine on soil nutritional properties depend on parent material, Ecosystems, 10(8), 1299-1310, 2007.

Teufel, B., Sushama, L., Arora, V., and Verseghy, D.: Impact of dynamic vegetation phenology on the simulated pan-Arctic land surface state, submitted to Climate Dynamics, 2017.

Timmons, D., Buchholz, T., and Veeneman, C. H.: Forest biomass energy: assessing atmospheric carbon impacts by discounting future carbon flows, GCB Bioenergy, 8, 631-643, 10.1111/gcbb.12276, 2016.

Verseghy, D. L., Mcfarlane, N. A., and Lazare, M.: CLASS - A Canadian land surface scheme for GCMs, II. Vegetation model and coupled runs, Int. J. Climatol., 13, 347-370, 1993.

Viovy, N.: CRU-NCEP reanalysis data version 4. Available at [http://dods.extra.cea.fr/store/p529viov/cruncep/V4_1901_2012/], (Accessed May 2015), 2012.

Wang, A., Price, D. T., and Arora, V. K.: Estimating changes in global vegetation cover (1850-2100) for use in climate models, Global Biogeochem. CycesCycles, 20, GB3028, 2006.

Wang, G., Sun, S., and Mei, R.: Vegetation dynamics contributes to the multi-decadal variability of precipitation in the Amazon region, Geophys. Res. Lett., 38, L19703, doi:10.1029/2011GL049017, 2011.

Wen, X., Tang, G., Wang, S., and Huang, J.: Comparison of global mean temperature series, Advances in Climate Change Research, 2, 187-192, 2011.

Wu, Y., Verseghy, D. L. and Melton, J. R.: Integrating peatlands into the coupled Canadian Land Surface Scheme (CLASS) v3.6 and the Canadian Terrestrial Ecosystem Model (CTEM) v2.0, Geosci Model Dev, 9(8), 2639–2663, doi:10.5194/gmd-9-2639-2016, 2016.

Zhang, Z., Xue, Y., Macdonald, G., Cox, P. M., and Collatz, G. J.: Investigation of North America vegetation variablilityvariability under recent climate: A study using the SSiB4/TRIFFID biophysical/dynamic vegetation model, J. Geophys. Res. Atmos., 120, 1300-1321, 2015.

Zhu, Z., Bi, J., Pan, Y., Ganguly, S., Anav, A., Xu, L., Samanta, A., Piao, S., Nemani, R. R., and Myneni, R. B.: Global data sets of vegetation leaf area index (LAI)3g and fraction of photosynthetically active radiation (FPAR)3g derived from global inventory modeling and mapping studies (GIMMS) normalized difference vegetation index (NDVI3g) for the period 1981- to 2011, Remote Sens., 5, 927-948, doi:10.3390/rs5020927, 2013.

Zobler, L.: A world soil file for global climate modelling, Tec. Rep. NASA TM-87802, 14-32, 1986.

Table 1: Plant functional types (PFTs) represented in CTEM and their relation to CLASS PFTs.

CLASS PFTs	**CTEM PFTs**	**CTEM PFT Symbol**
Needleleaf trees	Needleleaf Evergreen trees	NDL-EVG
	Needleleaf Deciduous trees	NDL-DCD
Broadleaf trees	Broadleaf Evergreen trees	BDL-EVG
	Broadleaf Cold Deciduous trees	BDL-DCD-CLD
	Broadleaf Drought/Dry Deciduous trees	BDL-DCD-DRY
Crops	C_3 Crops	CROP-C3
	C_4 Crops	CROP-C4
Grasses	C_3 Grasses	GRASS-C3
	C_4 Grasses	GRASS-C4

Table 2: Reclassification of the 17 MODIS land cover classes into the nine CTEM PFTs

SN	Items	Tree				Crop	Grass	Bare	Reference
		NDL EVG	NDL DCD	BDL EVG	BDL DCD				
1	Woody Savanna			0.1	0.4		0.25	0.25	Dai et al. (2001)
2	Water bodies							1	
3	Urban built up areas	0.05			0.05		0.1	0.8	Dai et al. (2001)
4	Savanna			0.05	0.3		0.4	0.25	Wang et al. (2006)
5	Permanent Wetlands						0.25	0.75	Dai et al. (2001)
6	Permanent snow and ice							1	Wang et al. (2006)
7	Open Shurblands	0.1			0.15		0.35	0.4	Wang et al. (2006)
8	Needleleaf evergreen	1							Wang et al. (2006)
9	Needleleaf deciduous		0.8				0.1	0.1	Wang et al. (2006)
10	Mixed forest	0.45			0.45		0.1		Wang et al. (2006)
11	Grasslands						0.65	0.35	Wang et al. (2006)
12	Croplands					0.9		0.1	Wang et al. (2006)
13	Cropland natural veg. mosaic			0.2		0.5	0.2	0.1	Wang et al. (2006)
14	Closed shrublands	0.2	0.2		0.4		0.2		Wang et al. (2006)
15	Broadleaf evergreen			1					Wang et al. (2006)
16	Broadleaf deciduous				1				Wang et al. (2006)
17	Bare ground							1	Wang et al. (2006)

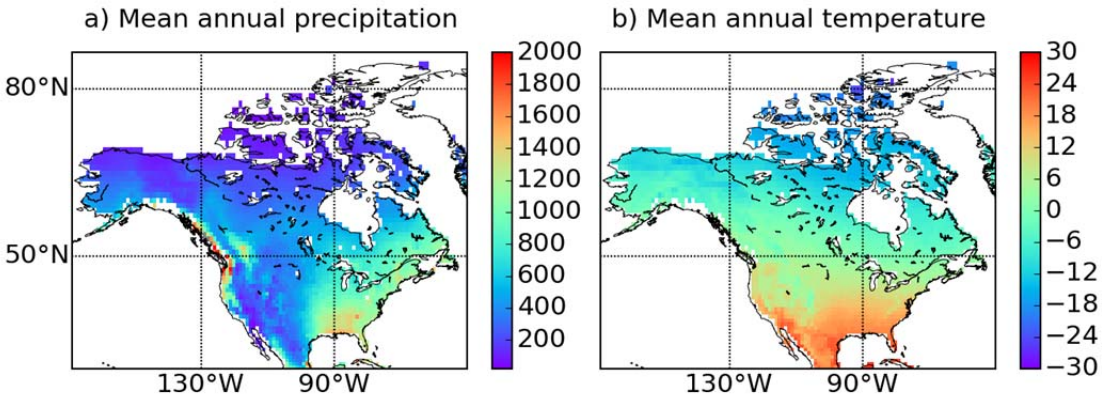

Figure 1. Spatial distribution of mean annual a) precipitation (mm), and b) temperature (°C) across North America. Grid cells with permanent ice/glaciers have been masked out.

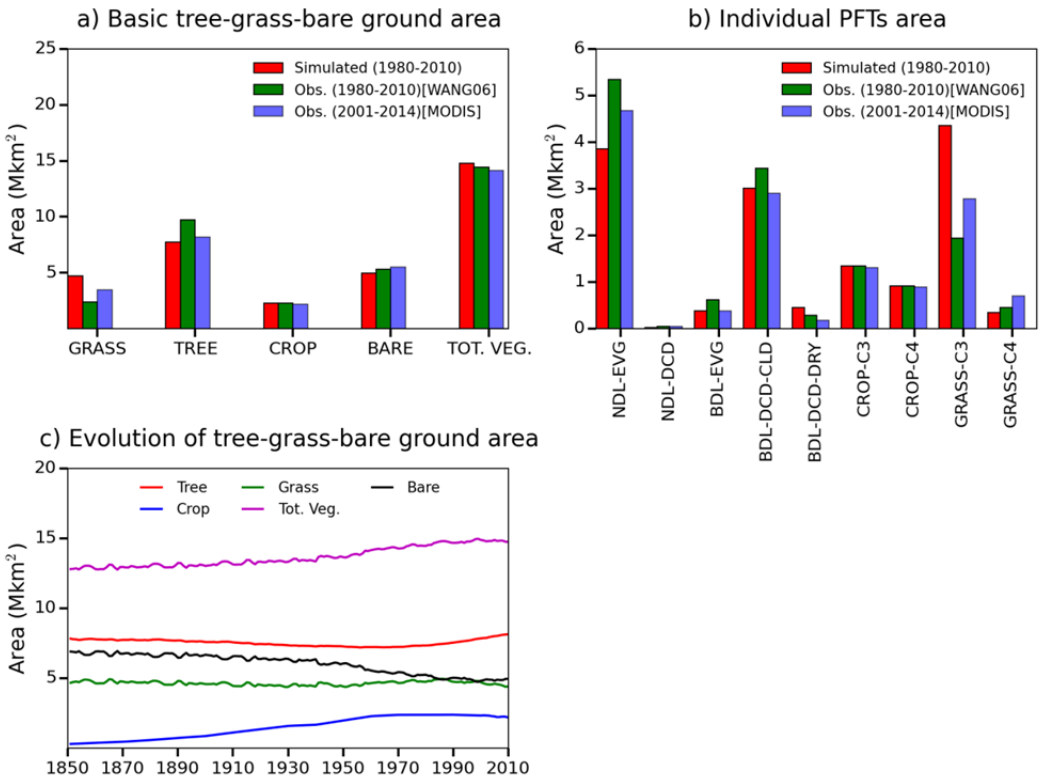

Figure 2. Comparison of observation-based and simulated vegetation areas summed over the North American domain a) grass, treed, crop, bare ground and total vegetated area, b) individual PFT areas, and c) evolution of simulated vegetation areas summed over the domain.

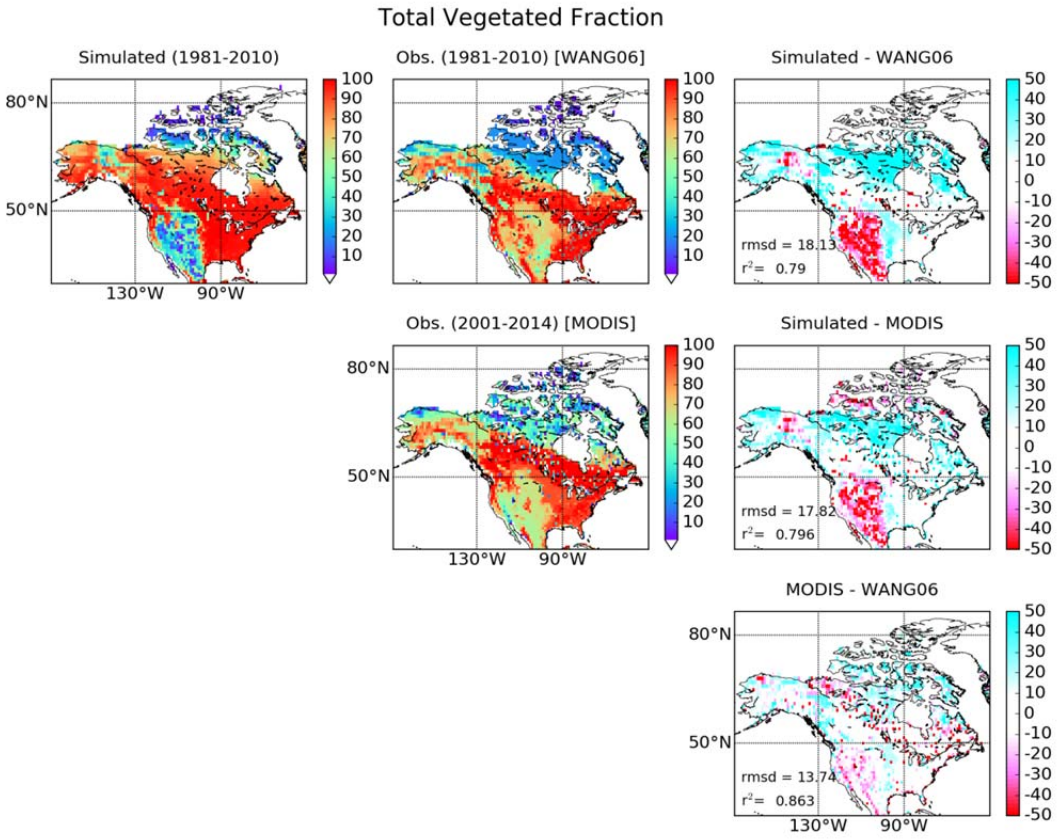

Figure 3. Spatial distribution of total vegetated coverage across North America. Simulated, observation-based, and differences are presented in the left, middle and right columns, respectively. The differences column includes model biases with respect to WANG06 (top panel) and MODIS (middle panel), and the difference between the two observation-based estimates (bottom panel). Root mean square difference (rmsd) and coefficient of determination (r^2) are also shown in each case.

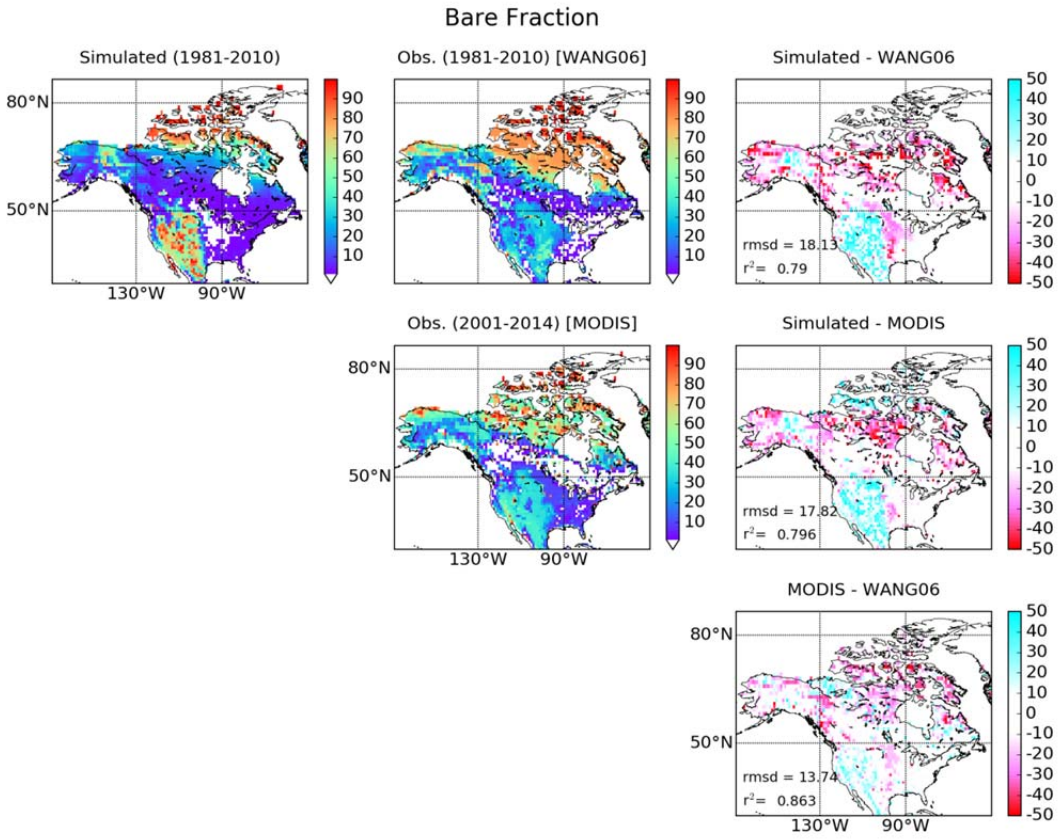

Figure 4. Spatial distribution of bare ground coverage across North America. Simulated, observation-based, and differences are presented in the left, middle and right columns, respectively. The differences column includes model biases with respect to WANG06 (top panel) and MODIS (middle panel), and the difference between the two observation-based estimates (bottom panel). Root mean square difference (rmsd) and coefficient of determination (r^2) are also shown in each case.

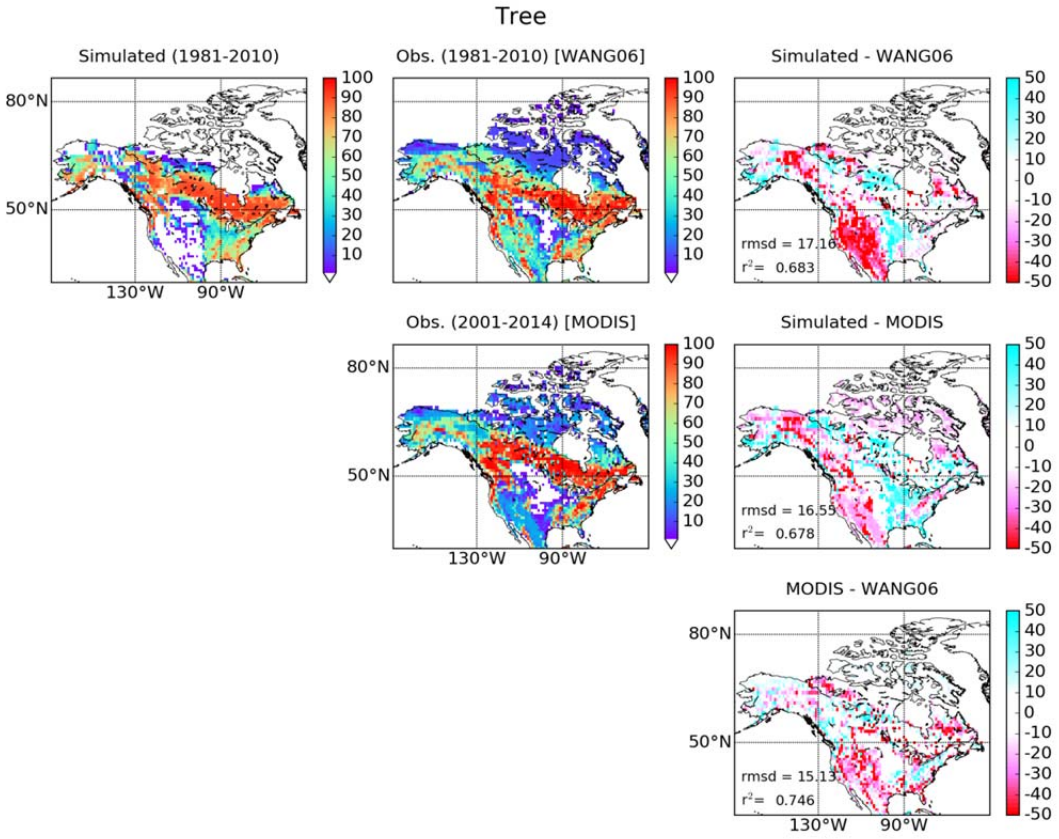

Figure 5. Spatial distribution of tree coverage across North America. Simulated, observation-based, and differences are presented in the left, middle and right columns, respectively. The differences column includes model biases with respect to WANG06 (top panel) and MODIS (middle panel), and the difference between the two observation-based estimates (bottom panel). Root mean square difference (rmsd) and coefficient of determination (r^2) are also shown in each case.

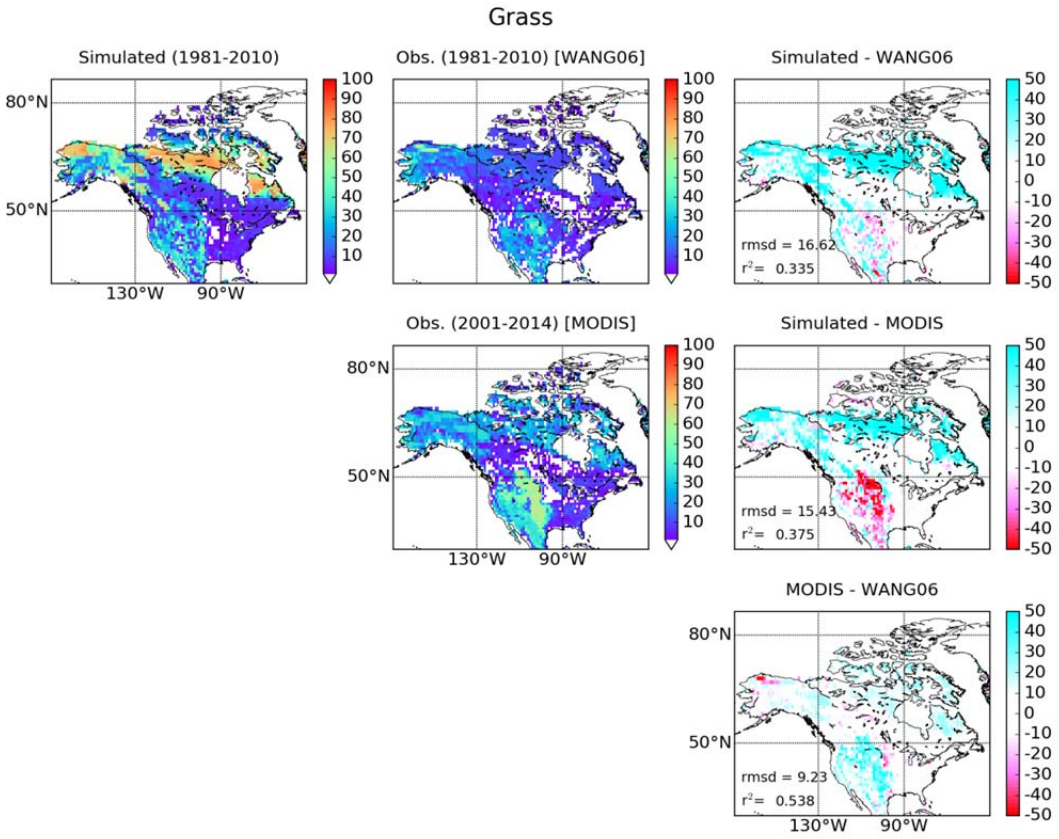

Figure 6. Spatial distribution of grass coverage across North America. Simulated, observation-based, and differences are presented in the left, middle and right columns, respectively. The differences column includes model biases with respect to WANG06 (top panel) and MODIS (middle panel), and the difference between the two observation-based estimates (bottom panel). Root mean square difference (rmsd) and coefficient of determination (r^2) are also shown in each case.

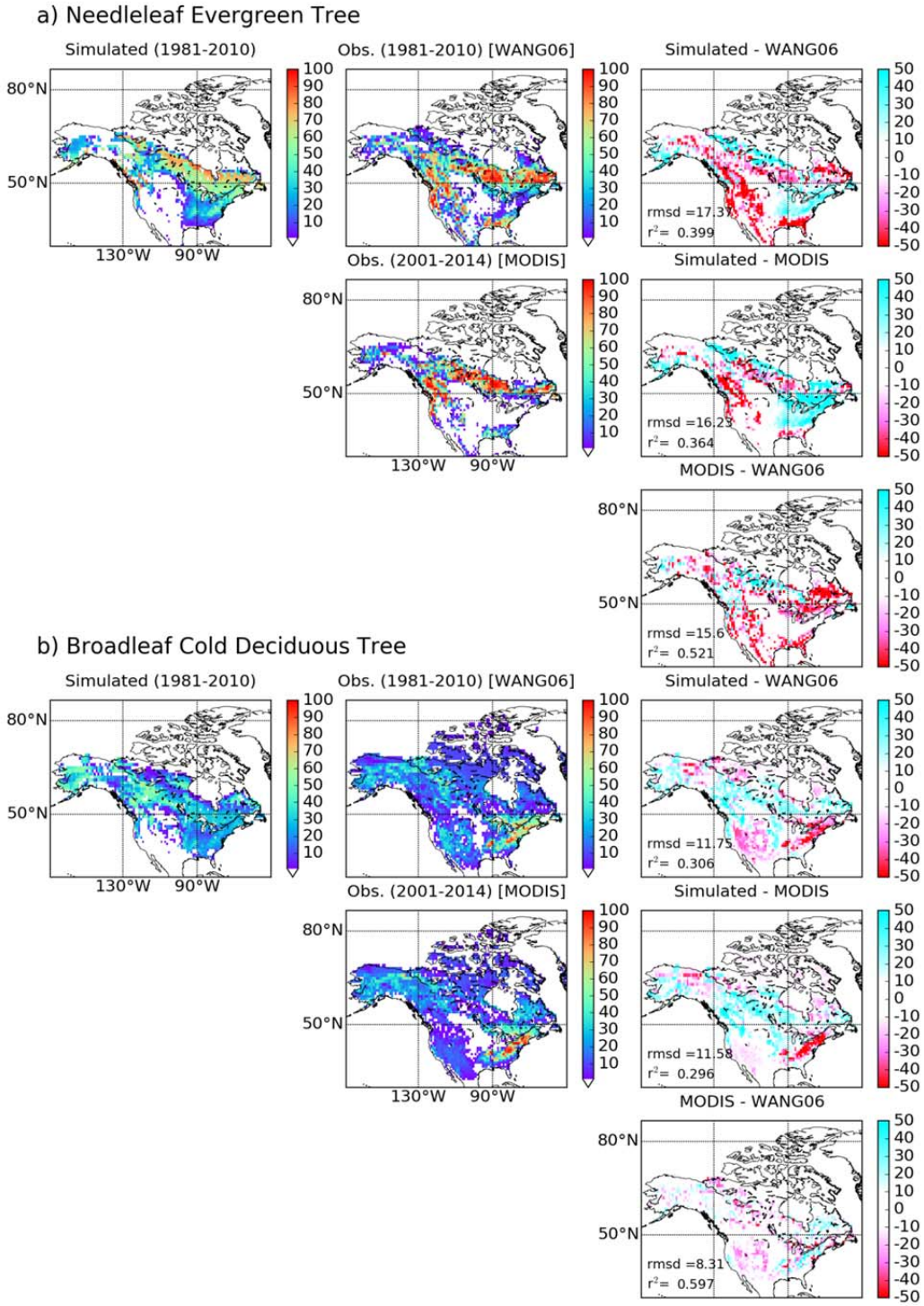

Figure 7. Spatial distribution of a) needleleaf evergreen tree, and b) broadleaf cold deciduous tree across North America. Simulated, observation-based, and differences are presented in the left, middle and right columns, respectively. The differences column includes model biases with respect to WANG06 (top panel) and MODIS (middle panel), and the difference between the observation-based estimates (bottom panel). Root mean square difference (rmsd) and coefficient of determination (r^2) are also shown in each case.

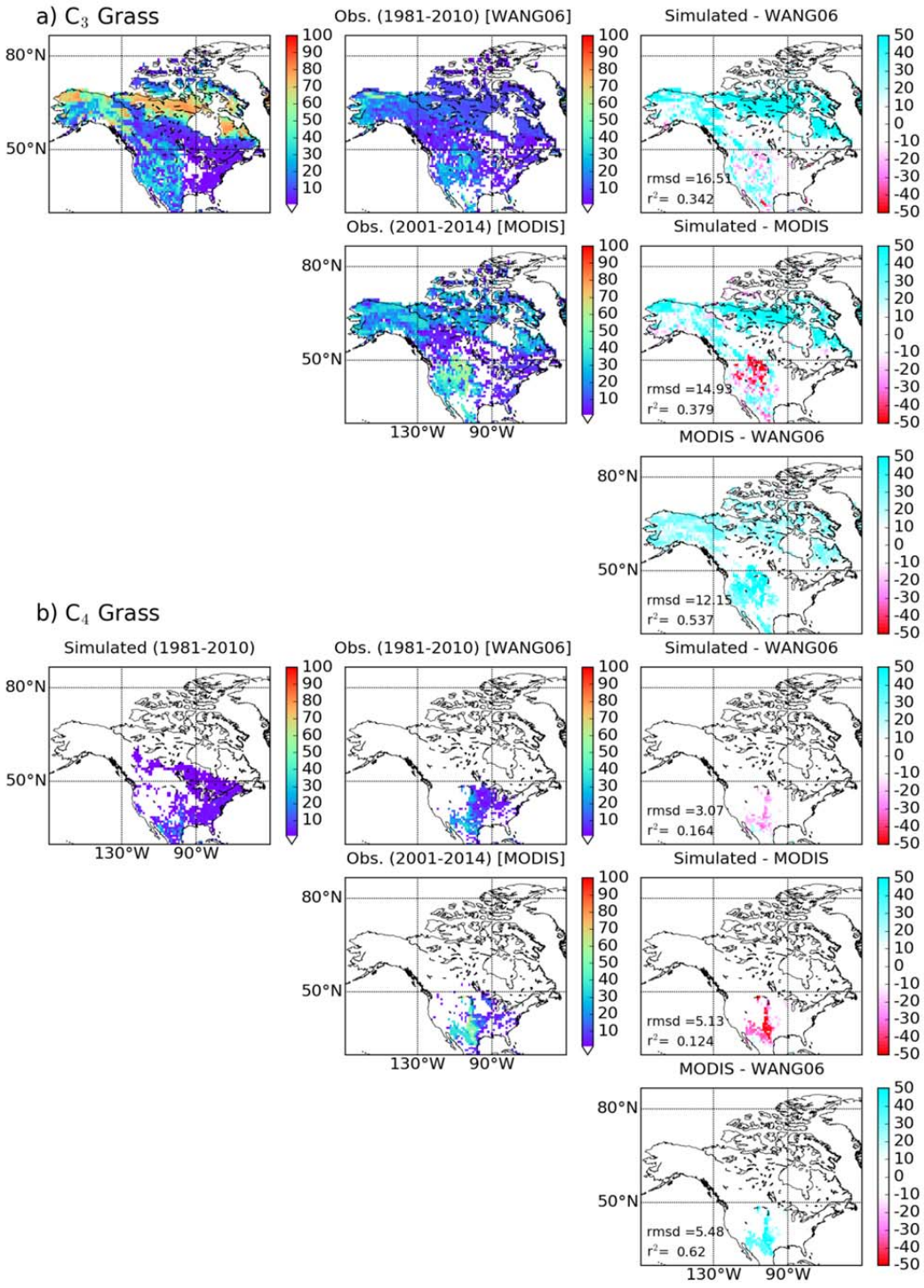

Figure 8. Spatial distribution of a) C_3 grasses, and b) C_4 grasses across North America. Simulated, observation-based, and differences are presented in the left, middle and right columns, respectively. The differences column includes model biases with respect to WANG06 (top panel) and MODIS (middle panel), and the difference between the the observation-based estimates (bottom panel). Root mean square difference (rmsd) and coefficient of determination (r^2) are also shown in each case.

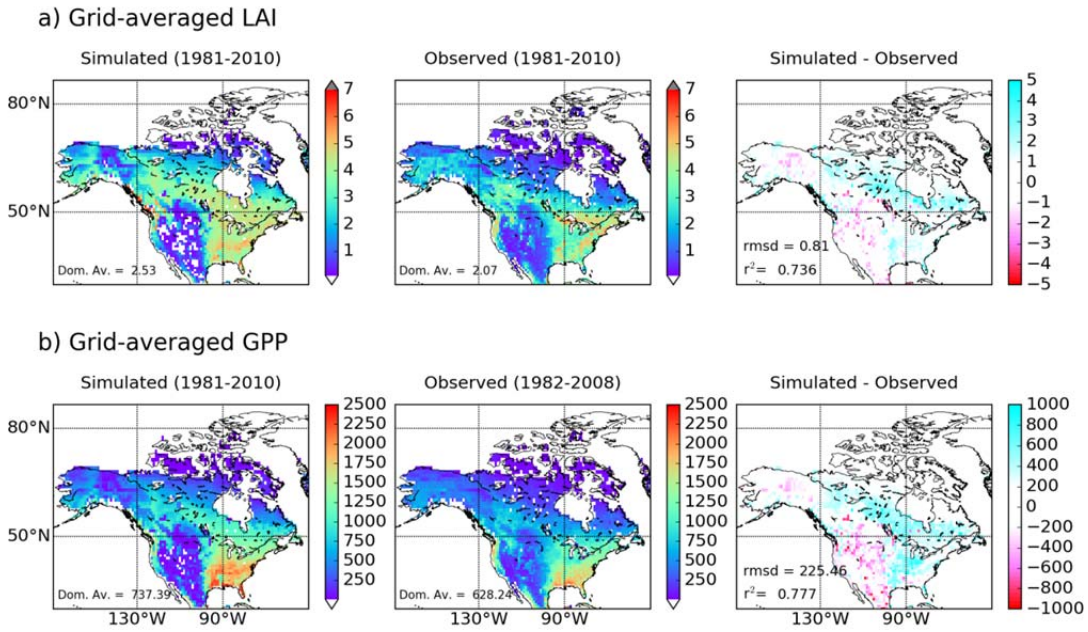

Figure 9. Spatial distribution of a) grid averaged maximum LAI (m^2 m^{-2}), and b) grid averaged GPP (g C m^2 y^{-1}) across North America. Simulated, observation-based, and differences between them are presented in the left, middle and right columns, respectively. Root mean square difference (rmsd) and coefficient of determination (r^2) are also shown in each case.

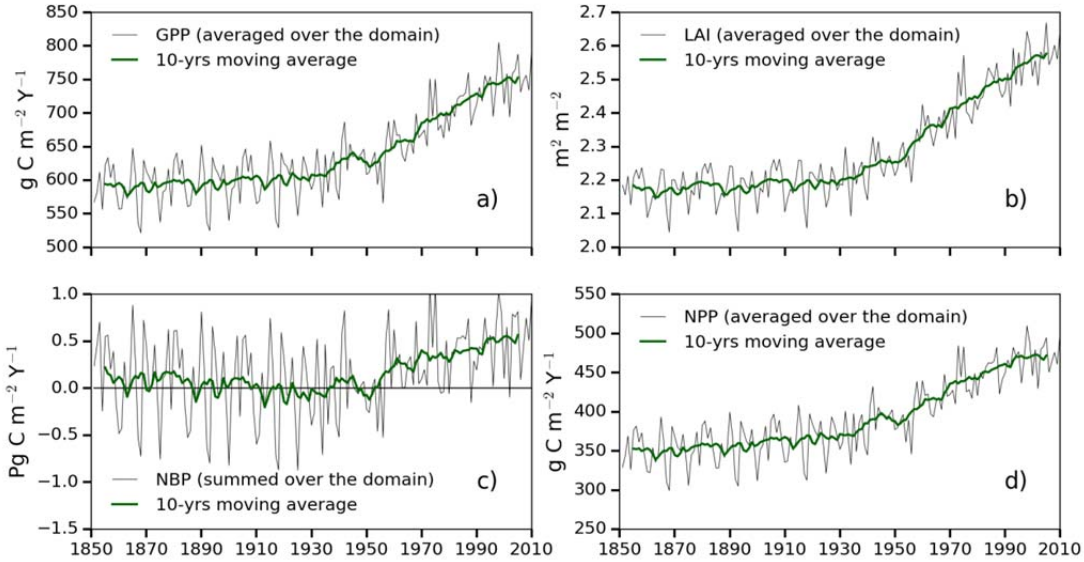

Figure 10. Time series evolution of a) domain averaged GPP (g C m^{-2} y^{-1}), b) domain averaged LAI (m^2 m^{-2}), c) domain total NBP (Pg C m^{-2} y^{-1}), and d) domain averaged NPP (g C m^{-2} y^{-1}).

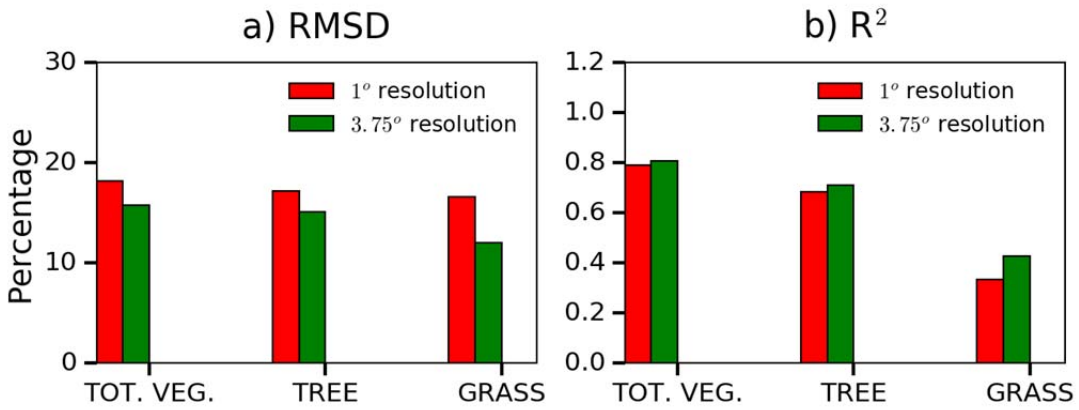

Figure 11. Comparison of the performance of the model at the 1° spatial resolution in this study with that at the 3.75° spatial resolution in the Melton and Arora (2016) study. The Melton and Arora (2016) global results were extracted for the North American domain. Spatial correlations and root mean square differences are used as metrics for the comparison between simulated and the observation-based estimate based on the modified WANG06 land cover product for fractional coverage of total vegetation, tree and grass.

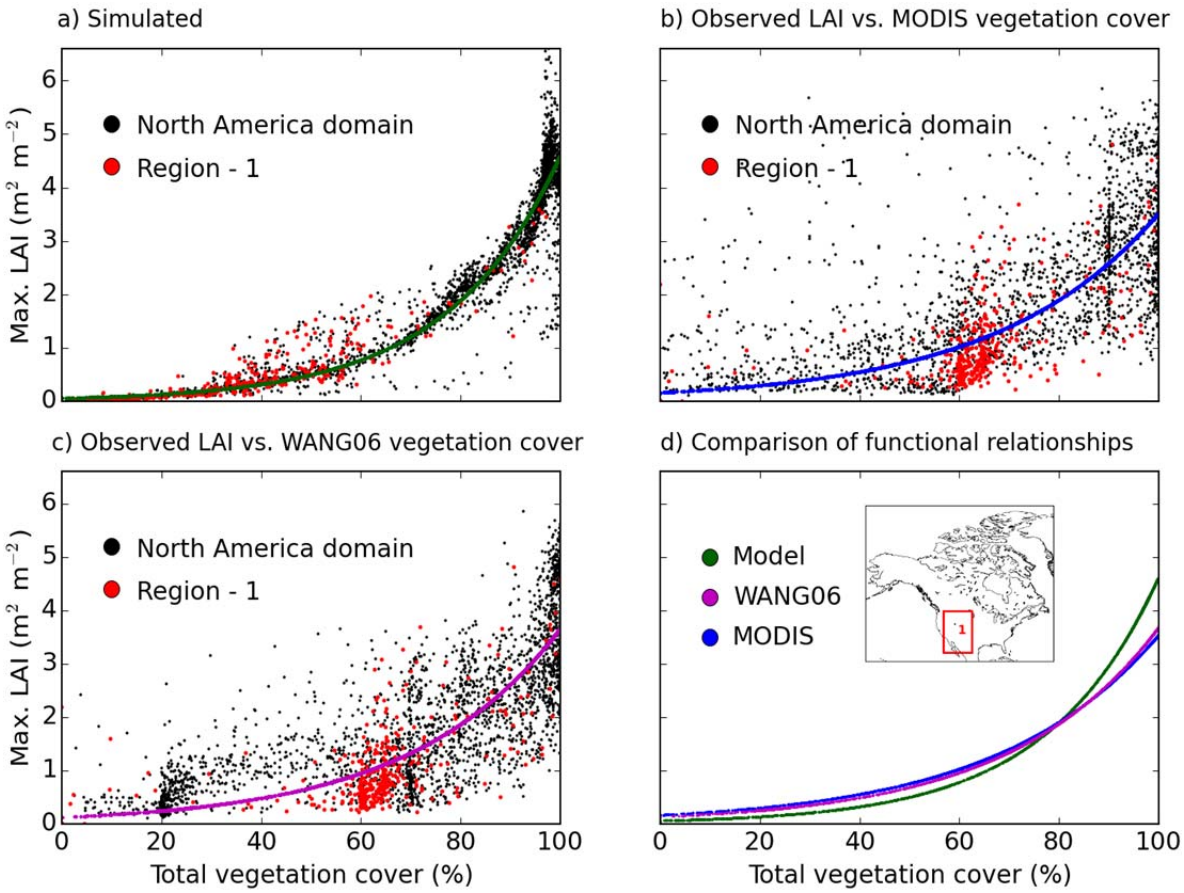

Figure 12. Scatter plots of a) simulated LAI vs. simulated total vegetation coverage, b) observed LAI vs. MODIS-derived total vegetation coverage, c) observed LAI vs. WANG06 total vegetation coverage. Plot d) shows a comparison of the fitted curves represented by solid lines, with an inset map of North America showing the sub-domain of interest bounded by a red rectangle.